A PSEUDO 3D VISCOELASTIC WINDING MODEL

by

Haowen Yu, Edmond Poh, J. Keith Good and Hongbing Lu
Oklahoma State University
USA

ABSTRACT

A pseudo 3D winding model that has considered orthotropic viscoelastic effects during winding and storage has been developed and implemented in a code revised from the 2D viscoelastic winding code developed by Qualls and Good [1]. The model discretizes the web into smaller segments of equal width, each having a constant web thickness within a segment. Tension is assigned to each segment using Hakiel's approach [2]; the tension is updated after the winding of each lap based on the deformed radius of the segment relative to the relaxed radius profile of that lap. In each segment, a 2D winding model is applied. The pseudo 3D model is capable of dealing with (1) a varying thickness profile in both CMD (cross machine direction) and MD (machine direction); (2) winding tension variation with the winding laps; and (3) varying core stiffness in the CMD. Moreover, with the consideration of viscoelastic behavior in the web the effects of winding conditions, such as winding speed and tension, on the wound roll stress can be determined. The model is especially suitable for viscoelastic materials with relatively short characteristic relaxation times, such as plastic webs with glass transition temperature close to room temperature. Numerical methods were used to determine the stress distributions in the wound roll. The pseudo 3D viscoelastic winding model was validated by comparing results on the dimensional changes of a web in three situations. They include (1) the formation of cambered web (in-plane imperfection) due to linearly varying thickness; and (2) the formation of localized baggy lanes due to an edge burr following slitting; and (3) the formation of baggy web (out-of-plane imperfection) due to increased web thickness in the middle of the web. Simulation results compare favorably with experimental data.

NOMENCLATURE

A	the amplitude of wavy edge, m
b	the width of a web, m
$\bar{h}$	the average web thickness, m
i	the lap numbers within the roll

j	widthwise position
$J_r(t)$	the radial creep function, 1/Pa
$J_\theta(t)$	the circumferential creep function, 1/Pa
$J_{r\theta}(t)$, $J_{\theta r}(t)$	the Poisson's creep function, 1/Pa
$Length_{burr}$	the length of deformed web at burr area, m
$Length_{rest}$	the length of deformed web at location other than the web edge, m
M	total number of widthwise locations
$r(i, j)$	the widthwise distribution of radius to the inside surface of lap i, j is the widthwise position, m
r_c	the outer radius of the core, m
$R_0(i)$	the relaxation radius of the lap i, radius at which the lap wound be stress free, m
T	the tension at the current lap, Pa
T_c	the tension at the core, Pa
T_f	the tension taper factor
$T(i)$	the actual winding tension force at lap *i,* N
$T_\theta(i)$	the predicted winding tension force at lap *i,* N
$\rho(i, j)$	widthwise radius distribution of wound roll, i is the lap number and j is the widthwise position, m
λ	the wave length, m
τ	the torque at current lap, N-m
τ_c	the torque at the core, N-m
ξ	the retardation time in generalized Kelvin Model, seconds

INTRODUCTION

Research focusing on stress analysis of wound rolls has received attention over decades. Most early winding models are two-dimensional elastic models. Detailed analysis of stresses in a 2D linear elastic wound roll perhaps began with the work of Gutterman [3] in 1959. Altman [4] followed Gutterman's work and presented an analytical solution to the linear elastic winding problem, including assumptions used and detailed derivation. The elastic model was extended by Yogoda [7] who included the potential for material orthotrophy and Pfeiffer [5, 6] who was the first to incorporate a radial modulus that was state dependent on pressure. In 1987, Hakiel [8] developed a practical numerical method that incorporated the advantages of the previous works. Moreover, in the Hakiel model both the state dependent radial modulus and orthotropic material properties were considered in formulation, and numerical solution was provided.

In order to investigate the viscoelastic effects in a wound roll, Tramposch [9, 10] introduced a 2D viscoelastic winding model in 1965. The web material was considered to be an isotropic viscoelastic material in his work. Lin and Westmann [11] extended Tramposch's work in viscoelastic winding mechanics by taking into account of histories for winding, winding-pause, and winding-pause-unwinding. Qualls and Good [1]

developed a solution for viscoelastic analysis that has considered viscoelastic effects after winding and the thermal effects on viscoelastic winding. The material in the Qualls-Good model is orthotropic with a nonlinear radial stiffness depending upon interlayer pressure.

All these models are 2D winding models and cannot be used to calculate the stress profile along CMD directly. In a wound roll, the stress and strain usually vary in both the radial and CMD directions. In some cases, the thickness variation becomes large enough that defects in the wound roll result. To account for the web thickness variation in a wound roll, three-dimensional winding models are needed for analysis of stress and strain for characterization of dimensional changes associated with defects such as cambered webs and non-flat (baggy) webs. Numerals 3D elastic winding models have been developed in the past. Hakiel [2] and Kedl [12] developed 3D winding models. They partitioned a roll into small strips or segments so that each segment can be considered as a 2D winding model. Hoffecker [13], and Lee and Wickert [14] developed 3D FEM elastic winding models to predict the width-wise variation of stresses in wound rolls and have compared the results with those obtained from previous models.

In this paper, a pseudo 3D viscoelastic winding model is presented. The variations in thickness and length in the CMD can be considered in this model. Viscoelastic effects during winding and storage have been considered in this model. Results and discussion will be given on the effects of thickness variations along CMD and winding tension variation with the winding laps. Some results are compared with the experimental data for validation.

PSEUDO 3D WINDING MODEL

In our work, we use the approach by Hakiel [2] to partition a 3D wound roll into a number of 2D segments. Some modifications will be made to the Hakiel model and the orthotropic material behavior will be considered.

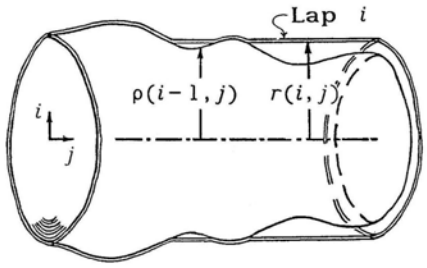

Figure 1 – Exaggerated view of a wound roll with thickness variation, Hakiel [2]

As shown in Figure 1, before the lap i is wound on the roll, the widthwise radius distribution of the wound roll is $\rho(i-1, j)$. Consider that the surface of wound roll is no longer cylindrical due to thickness variation and the winding tension is not high enough nor is the radial modulus low enough to result in large deformations. The lap i may or may not be in full contact with the wound roll surface. In the areas where the contact is made between the lap i and the wound roll, the radius of inside surface of lap i $r(i, j)$ is equal to the radius of the previous wound roll surface $\rho(i-1, j)$. In the areas where there is no contact, it will be assumed that the radius of inside surface of lap i $r(i, j)$ is constant and is equal to the relaxation radius $R_0(i)$ which is assumed as the inner radius of

a non-stretched part of the web. In order to determine the relaxation radius, the summation of tension applied on all segments at the current outer lap is set to be equal to the web tension.

$$T_\theta(i) = T(i) \qquad \{1\}$$

The predicted winding tension force is equal to the summation of tension force in all the widthwise positions.

$$T_\theta(i) = \sum_{j-1}^{M} \{\sigma_\theta(i,j)\frac{b\bar{h}}{M}\} = \frac{E_\theta b\bar{h}}{M(1-\nu_{r\theta}\nu_{\theta r})}\sum_{j-1}^{M}\{\frac{r(i,j)-R_0(i)}{R_0(i)}\} \qquad \{2\}$$

Usually, equation {1} cannot be satisfied the first time. However, in an iterating process, the relaxation radius $R_0(i)$ can be determined by extrapolating over previous estimates until the calculated winding tensile force is equal to the applied tensile force at the current radius and the tension in each widthwise position can be determined.

The inner radius of the lap being wound on is

$$r(i,j) = Max\{\rho(i-1,j), R_0(i); j = 1,...M\} \qquad \{3\}$$

The widthwise radius distribution of wound roll is

$$\rho(i,j) = r(i,j) + h(j); j = 1,...M \qquad \{4\}$$

Based on equations {1} ~ {4} the widthwise distribution of radius and tension can be determined at a designated wound roll radius. After that, the wound roll can be divided into several small segments at each layer. In each segment, a 2D viscoelastic winding model is applied to determine the time-dependent stress distributions in the segment. The models for the winding and storage will be discussed in the following sections separately.

VISCOELASTIC EFFECTS DURING WINDING

In this section, viscoelastic effects during winding will be considered and discussed. For viscoelastic materials with relatively short characteristic relaxation times, comparable to the time it takes to wind a roll, it is necessary to consider the viscoelastic effects during winding.

This part of work is based on the 2D viscoelastic winding model developed by Qualls and Good [1]. In the Qualls-Good model viscoelastic effects are considered after winding is finished. Their model has been extended in this paper to allow the consideration of viscoelastic effects from the beginning of the winding. With the consideration of viscoelastic effects during winding, some winding conditions, such as the winding velocity and winding tension as a function of radius or time can be considered.

Consider an orthotropic viscoelastic material with radial modulus depending on radial stress in 2D case in polar coordinates. The equilibrium equation is

$$r\frac{\partial\sigma_r}{\partial r} + \sigma_r - \sigma_\theta = 0 \qquad \{5\}$$

The strain compatibility in the rθ dimensions is given by:

$$r\frac{\partial \varepsilon_\theta}{\partial r} + \varepsilon_\theta - \varepsilon_r = 0 \qquad \{6\}$$

It should be noted that there is no strain compatibility enforced between segments. The constitutive equations for an orthotropic viscoelastic material are

$$\varepsilon_r = \int_0^t \left[J_r(t-t')\frac{\partial \sigma_r}{\partial t'} + J_{r\theta}(t-t')\frac{\partial \sigma_\theta}{\partial t'} \right] dt'$$

$$\varepsilon_\theta = \int_0^t \left[J_\theta(t-t')\frac{\partial \sigma_\theta}{\partial t'} + J_{\theta r}(t-t')\frac{\partial \sigma_r}{\partial t'} \right] dt' \qquad \{7\}$$

By solving equation {5}, σ_θ can be expressed in terms of σ_r as shown in equation {8}.

$$\sigma_\theta = r\frac{\partial \sigma_r}{\partial r} + \sigma_r \qquad \{8\}$$

We next insert equation {8} into equation {7} to eliminate σ_θ, and then substitute ε_θ, ε_r in equation {6} to obtain

$$\int_0^t [J_\theta(t-t')\frac{\partial}{\partial t'}(r^2\frac{\partial^2 \sigma_r}{\partial r^2}) + \{3J_\theta(t-t') + J_{\theta r}(t-t') - J_{r\theta}(t-t')$$

$$+ r\frac{\partial}{\partial r}J_\theta(t-t')\}\frac{\partial}{\partial t'}(r\frac{\partial \sigma_r}{\partial r}) + \{r\frac{\partial}{\partial r}(J_\theta(t-t') + J_{\theta r}(t-t')) + J_\theta(t-t')$$

$$+ J_{\theta r}(t-t') - J_r(t-t') - J_{r\theta}(t-t')\}\frac{\partial \sigma_r}{\partial t'}]dt' = 0 \qquad \{9\}$$

Qualls and Good [1] suggested that both J_θ and $J_{\theta r}$ are radially independent. Moreover $J_{\theta r} = J_{r\theta}$, therefore the equation {9} can be simplified as

$$\int_0^t \left[F_1(t-t')\frac{\partial}{\partial t'}(r^2\frac{\partial^2 \sigma_r}{\partial r^2}) + F_2(t-t')\frac{\partial}{\partial t'}(r\frac{\partial \sigma_r}{\partial r}) + F_3(t-t')\frac{\partial \sigma_r}{\partial t'} \right] \cdot dt' = 0 \qquad \{10\}$$

where $F_1(t-t') = J_\theta(t-t')$;

$F_2(t-t') = 3J_\theta(t-t')$;

$F_3(t-t') = J_\theta(t-t') - J_r(t-t')$.

J_r and J_θ follow the generalized Kelvin model. It should be noted that J_r is also a function of the radial pressure. The generalized Kelvin model is expressed as

$$J(t) = J_0 + \sum_{i=1}^{N} J_i (1 - e^{-t/\xi_i}) \qquad \{11\}$$

In order to solve equation {10}, a general form is assumed.

$$I = \int_0^t F(t-t') \frac{\partial f}{\partial t'} \cdot dt' \qquad \{12\}$$

As shown in Figure 2, for a wound roll with *n* laps we divide the entire winding time into n time steps. We have $t = t_k$ after winding lap *k* (radius $r = r_k$, $1 \le k < j \le n$). Therefore, at the current outer layer, lap *j*, $t = t_j$.

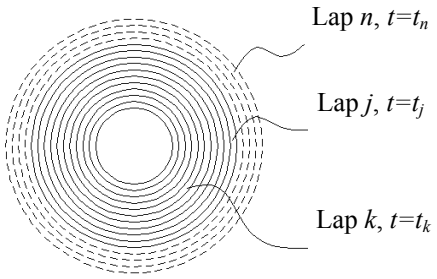

Figure 2 – Viscoelastic effects during winding

For the case of constant velocity $v(t) = v_0$, the time increment from t_j to t_k can be derived as follows.

Since $2\pi \int_{r_k}^{r_j} R \cdot dR = h \int_0^{\Delta t} v_0 \cdot dt$, we have

$$\Delta t = t_j - t_k = \frac{\pi \cdot \left(r_j^2 - r_k^2\right)}{v_0 h} \qquad \{13\}$$

And the integral I can be written as

$$I_j = F(t_j - t_{j-1}) \cdot \Delta f_j + F(t_j - t_{j-2}) \cdot \Delta f_{j-1} + \cdots + F(t_j - t_{k-1}) \cdot \Delta f_k \qquad \{14\}$$

where $\Delta f_j = f_{t=j} - f_{t=j-1}$. Thus $\Delta f_{j-1}, \Delta f_{j-2}, \ldots, \Delta f_k$ are already known when $t = t_j$. And $F(t_j - t_{j-1}), F(t_j - t_{j-2}), \ldots, F(t_j - t_{k-1})$ can be calculated at any radius using the formula for the creep compliance. Thus the only unknown is Δf_j.

Comparing equation {10} and {12}, we can find that the function *f* could be either $r^2 \frac{\partial^2 \sigma_r}{\partial r^2}$, or $r \frac{\partial \sigma_r}{\partial r}$, or σ_r. Therefore Δf_j (the increment of *f* from $t = t_{j-1}$ to $t = t_j$)

can be expressed in terms of $r^2\frac{\partial^2\Delta\sigma_r}{\partial r^2}, r\frac{\partial\Delta\sigma_r}{\partial r}$ or $\Delta\sigma_r$, where Δ refers to the increment from $t=t_{j-1}$ to $t=t_j$. After using equation {15}, Δf_j can be rewritten in terms of $\Delta\sigma_{r(k+1)}, \Delta\sigma_{r(k)}, \Delta\sigma_{r(k-1)}$.

$$\frac{\partial^2\Delta\sigma_r}{\partial r^2}\approx\frac{\Delta\sigma_{r(k+1)}-2\Delta\sigma_{r(k)}+\Delta\sigma_{r(k-1)}}{h^2}$$

$$\frac{\partial\Delta\sigma_r}{\partial r}\approx\frac{\Delta\sigma_{r(k+1)}-\Delta\sigma_{r(k-1)}}{2h} \qquad \{15\}$$

Then the general form *I* in equation {12} can be represented by $\Delta\sigma_{r(k+1)}, \Delta\sigma_{r(k)}, \Delta\sigma_{r(k-1)}$. At radius $r=r_k$, equation {10} will be represented by a general form.

$$G_k(\Delta\sigma_{r(k+1)}, \Delta\sigma_{r(k)}, \Delta\sigma_{r(k-1)})=0 \quad (k=1,2,...j-1) \qquad \{16\}$$

Equation {16} can be written for each radial location within the wound roll. When $t=t_j$ there are *j-1* simultaneous algebraic equations with *j+1* unknowns. After both the outer and inner boundary conditions at $t=t_j$ are applied, this system of equations can be solved.

VISCOELASTIC EFFECTS AFTER WINIDNG

After winding process is finished, the total number of laps is n. For radius $r=r_k$, at time $t=t_m\ (n<m)$, the integral I can be written as

$$I_m=F(t_m-t_{m-1})\cdot\Delta f_m+F(t_m-t_{m-2})\cdot\Delta f_{m-1}+\cdots+F(t_m-t_{k-1})\cdot\Delta f_k \qquad \{17\}$$

where $\Delta f_m=f_{t=m}-f_{t=m-1}$. When $t=t_m$, $\Delta f_{m-1}, \Delta f_{m-2}, \ldots, \Delta f_k$ are already known. $F(t_m-t_{m-1}), F(t_m-t_{m-2}), \ldots, F(t_m-t_{k-1})$ can be calculated at any radius using the formula for the creep compliance. Thus the unknown is Δf_m only when $t=t_m$.

Substitution of the finite difference approximation gives

$$\frac{\partial^2\Delta\sigma_r}{\partial r^2}\approx\frac{\Delta\sigma_{r(k+1)}-2\Delta\sigma_{r(k)}+\Delta\sigma_{r(k-1)}}{h^2}$$

$$\frac{\partial\Delta\sigma_r}{\partial r}\approx\frac{\Delta\sigma_{r(k+1)}-\Delta\sigma_{r(k-1)}}{2h} \qquad \{18\}$$

Similarly, at radius $r = r_k$, the relation among $\Delta\sigma_{r(k+1)}, \Delta\sigma_{r(k)}, \Delta\sigma_{r(k-1)}$ can be written in terms of a general form as follows:

$$H_k(\Delta\sigma_{r(k+1)}, \Delta\sigma_{r(k)}, \Delta\sigma_{r(k-1)}) = 0 \quad (k=1,2,...n-1) \qquad \{19\}$$

Equation {19} can be written for each radial location within the wound roll. At $t = t_m$, there are *n-1* simultaneous algebraic equations with *n+1* unknowns. When both the outer and inner boundary conditions at $t = t_m$ are applied, this system of equations can be solved.

RESULTS AND DISCUSSIONS

As mentioned in previous sections, the pseudo 3D viscoelastic winding model is capable of dealing with the thickness variation in both CMD and MD directions, as well as winding tension variation with the winding laps. In this section, some validation results will be presented for the pseudo 3D viscoelastic winding model.

We created CMD thickness variations in the winding experiment by adding a stack of web strips of the same web material being wound at every nth lap [17]. In addition, in the numerical calculation all the extra thickness and related volume are assumed to be allocated evenly in these n laps. Therefore, in these several laps, the thickness varies only in the CMD direction and the thickness profile is persistent in the MD direction. In this part, three special cases have been considered: (1) The formation of cambered web due to linearly varying thickness; (2) The formation of localized baggy lanes due to edge burr following slitting; and (3) The formation of baggy web due to thickness increment in the middle of the web. The simulation results using the pseudo 3D viscoelastic winding model will be compared with experimental data and the deformation results from pseudo 3D viscoelastic winding model. The dimensional changes estimated by numerical simulations will be compared with measured data.

After the pseudo 3D viscoelastic winding model is validated by three special cases. We will focus on the second aspect, winding tension variation with the winding laps only. The tension taper factor was introduced based the work by Shelton [15] and Feiertag [16] and implemented into pseudo 3D viscoelastic winding code. For each tension taper factor, the winding tension and torque are varying with the winding laps. The stress results will be given for the tension taper factor from 0 to 1. The effect of winding tension variation can be determined based on the numerical results. There are no experimental results available for this part.

The material used in the three cases is polyethylene web of 63.5 μm (2.5 mil) thick and 15.24 cm (6 in) wide. The in-plane and out-of-plane creep compliance data are taken from Qualls and Good [1]. The out-of-plane creep compliance follows

$$J_r(t) = \frac{1}{167.24\sigma_r - 0.09855\sigma_r^2 - 0.000422\sigma_r^3} + 3.058\times10^{-5} - 2.034\times10^{-5}\cdot e^{-t/2.78\times10^3} - 1.024\times10^{-5} e^{-t/2.613\times10^5}$$

The in-plane creep compliance follows

$$J_\theta(t) = \frac{1}{24000} + 1.62\times10^{-4} - 1.285\times10^{-5}\cdot e^{-t/1\times10^4} - 1.491\times10^{-4} e^{-t/1\times10^7}$$

where σ_r has units of psi, t is in seconds and $J_r(t)$ is in 1/psi in these in-plane and out-of-plane creep compliance data.

Case One: Formation of a Cambered Web

A CMD thickness variation was created during winding by adding a stack of 3 inserts of equilateral triangular webs at every fourth lap. The schematic of this insertion is shown in Figure 3. While using the pseudo 3D winding model, the web was divided into ten small segments. Since the pseudo 3D winding model is an axisymmetric model, it is assumed that for each 2D segment the extra thickness and associated volume will be allocated evenly in these four laps respectively. From location #1 to #10, the thickness increases linearly.

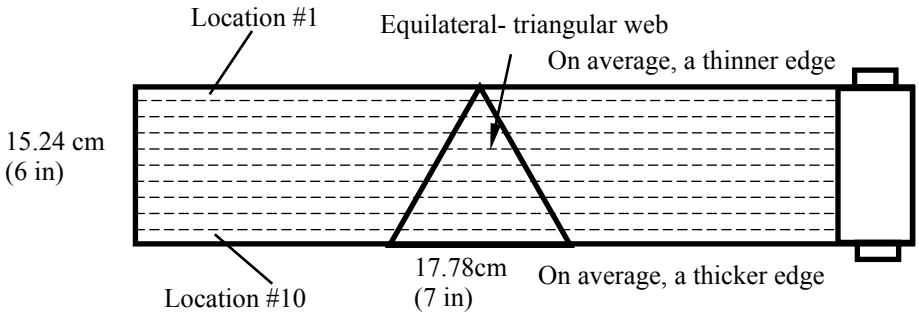

Figure 3 – Schematic diagram for inserting a triangular web for every four plies for use in the investigation of formation of a cambered web

The pseudo 3D viscoelastic winding model has been used to simulate this viscoelastic winding problem. The winding speed is 1.31 m/min (4.3 ft/min) and winding tensile stress is 2.99 MPa (433.3 psi). The total wound roll length is around 22.2 m (72 ft 10 in) and the number of laps is 110 layers. The storage time is 86400 seconds (24 hours). The length of deformed web at the ten locations is obtained using the pseudo 3D winding model and is plotted in Figure 4.

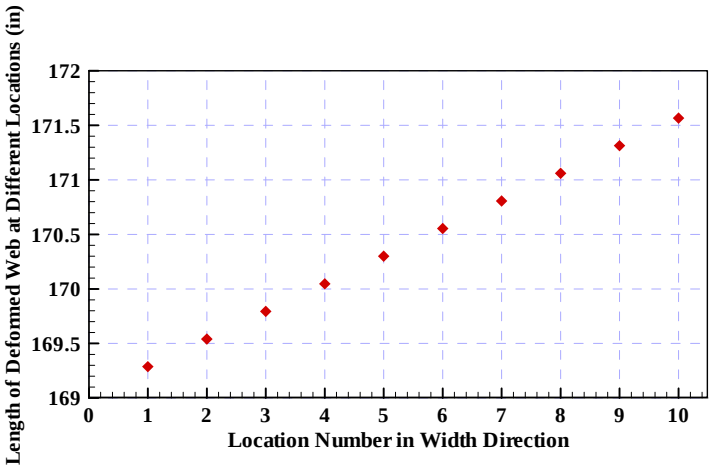

Figure 4 – The length of deformed web at ten locations

From the data shown in Figure 4, we can find that the length of deformed web changes linearly along the CMD direction as shown in Figure 5I. Since the web edges

are straight in a cambered web, results in Figure 5I can be plotted as shown in Figure 5II, with the use of an appropriate radius and central angle as shown in Figure 5III.

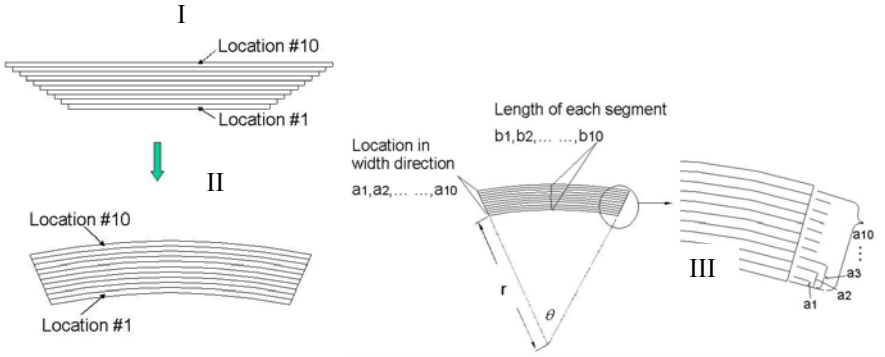

Figure 5 – Numerical transformation for cambered web

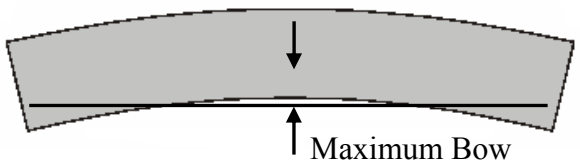

Figure 6 – Maximum bow length

In Figure 5, b_1, b_2, ..., b_{10} represent the lengths of segments. a_1, a_2, …, a_{10} stand for the distances from inner edge to the upper edge of these segments. They satisfy the following equations

$$\begin{cases} (r+a_1)\cdot\theta = b_1 \\ (r+a_2)\cdot\theta = b_2 \\ \vdots \\ \vdots \\ (r+a_{10})\cdot\theta = b_{10} \end{cases} \quad \{20\}$$

In this case, the numerical simulation gives the results r =10.18 m (400.83 in) and θ = 24.18 degrees (0.422 radians). Therefore, we can obtain the maximum bow length as shown in Figure 6 is around 0.226 m (8.89 in). The value of maximum bow length from experiment is 0.191 m (7.5 in). The deformed shapes of web at ten locations are simulated and shown in Figure 7. The numerical results and experimental data are in same order of magnitude though there are still some errors.

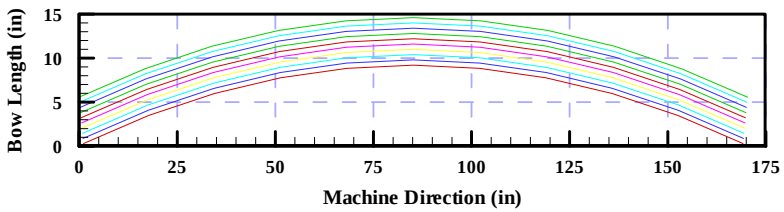

Figure 7 – Deformed shape after storage

Case Two: Formation of a Wavy Edge

A web with a wavy edge is primarily the result of winding a web with an edge burr following slitting. The setup is shown in Figure 8. The segment close to one edge is thicker than the other segments. The web sample cross-section was viewed observed under a microscope to acquire the image of the web edge and is also shown in Figure 8. The thickness profile is assumed to be persistent along MD.

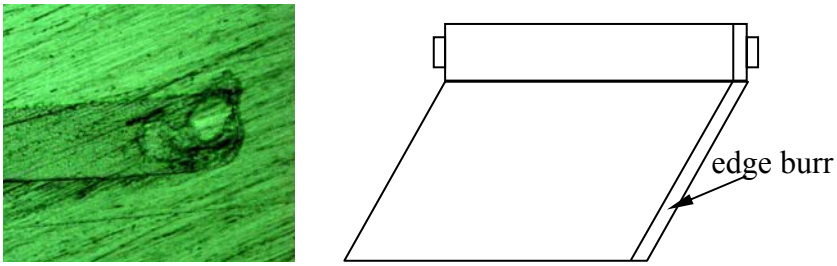

Figure 8 – Formation of wavy edge

The pseudo 3D viscoelastic winding model was used to simulate this wavy edge problem. As mentioned before, the material used is polyethylene web of 63.5 μm (2.5 mil) thick and 15.24 cm (6 in) wide. The height of edge burr is 20.4 μm (0.803 mil) and the winding tensile stress is 2.07 MPa (300 psi). The number of laps is 80. The storage time is 86400 seconds (24 hours). The length of deformed web at ten locations is plotted in Figure 9.

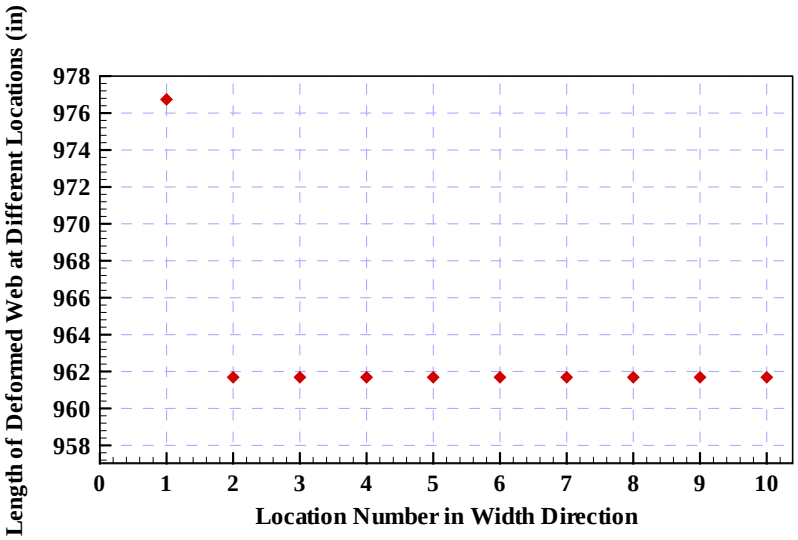

Figure 9 – The length of deformed web at ten locations

As shown in Figure 9, the deformation in the edge burr area is much larger than the rest of the web. The deformations in the rest of the web are constant. In the experiment, we observed the wavy edge and found that the wavy edge follows approximately a sinusoidal oscillation. Therefore, we assume that the deformed shape follows equation {21} at the edge burr, and the deformation of web can be converted from shape I into shape II as depicted in Figure 10.

$$y = A \cdot \sin(\frac{2\pi x}{\lambda}) \qquad \{21\}$$

where λ is the wave length, A is the amplitude of wavy edge. These two parameters can be determined in numerical simulation and measured in experiment. Then the shape of wavy edge can be simulated and examined.

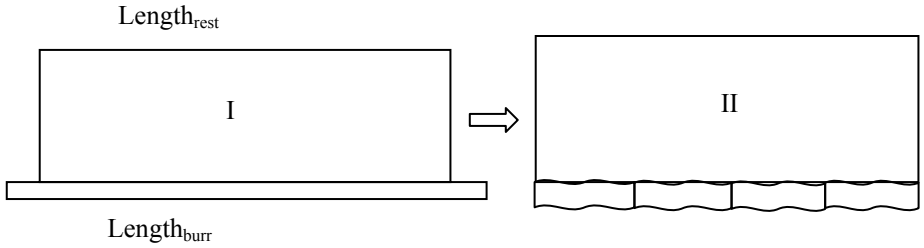

Figure 10 – Numerical transformation for wavy edge

In the experiment, the wave length and amplitude have been obtained through image analysis. λ is 2.34 cm (0.923 in) and the A is 0.794 mm (31.26 mil). In the numerical simulation, the wave length (λ) and amplitude (A) were extracted from equation {22}.

$$\frac{Length_{burr}}{Length_{rest}/\lambda} = \int_0^{\lambda} \sqrt{1 + \frac{4\pi^2 A^2}{\lambda^2} \cos^2\left(\frac{2\pi x}{\lambda}\right)} dx \qquad \{22\}$$

It is assumed that the wavy edge has the same wavy length as that in the experiment to determine the amplitude. Based on equation {22}, the amplitude of wavy edge can be determined. In this numerical simulation, the amplitude is determined as 0.939 mm (36.96 mil) based on the deformation results from the pseudo 3D winding model and wavy length data from experiment. The numerical results and experimental data are in the same order although there are still some errors.

Case Three: Formation of Baggy Web

In this case, CMD thickness variation was generated by adding a stack of 6 inserts of strip webs at every sixth lap. The example setup is shown in Figure 11. In the pseudo 3D winding model, the web was divided into forty segments. Since the pseudo 3D winding model is an axisymmetric model, it is assumed that the extra thickness and volume will be allocated evenly in these six laps at each location respectively. The segments at the middle of web are thicker that the rest.

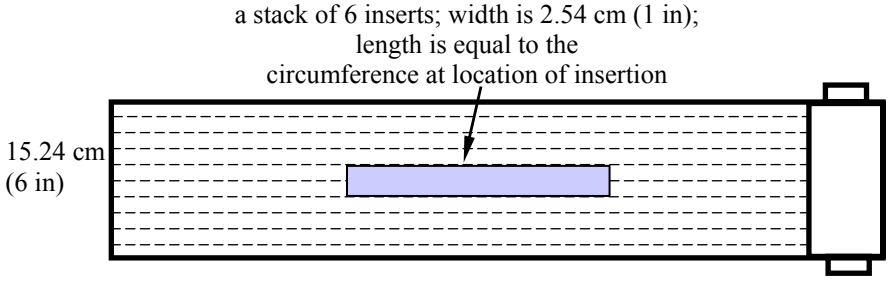

Figure 11 – Formation of baggy web

The pseudo 3D viscoelastic winding model has been used to simulate this baggy web problem. The winding speed is 1.31 m/min (4.3 ft/min) and the winding tensile stress is 2.30 MPa (333.3 psi). The number of laps is around 50. The storage time is 108000 seconds (30 hours). The lengths of deformed web at forty locations determined from simulations are plotted in Figure 12.

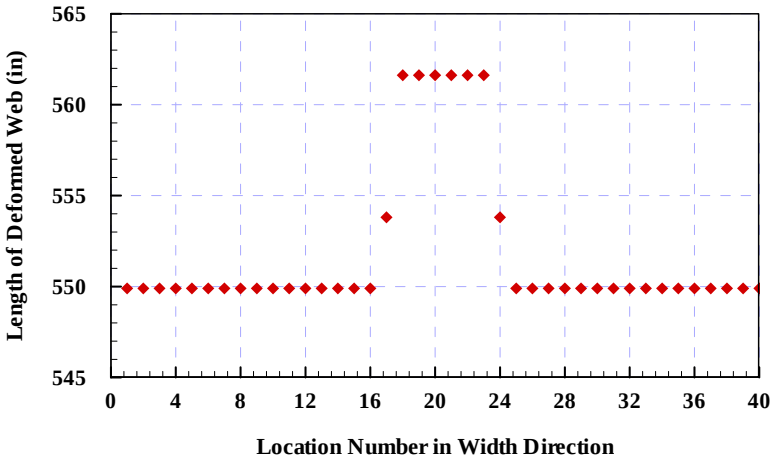

Figure 12 – The lengths of deformed web at forty locations

From results shown in Figure 12, the lengths of deformed web reach the maximum value at the middle segments. Results are quantified in this example in terms of h as shown in Figure 13, a measure of the out-of-plane deformation of the web that resulted from the thickness variation. The amplitude of h is expressed by equation {23}. Numerical solution for h, based on the model results was 0.948 mm. The experimental result for h is 0.7 mm. The numerical results and experimental data are within the same order of magnitude. Based on the numerical solution, the deformed shape of wound roll is shown in Figure 14.

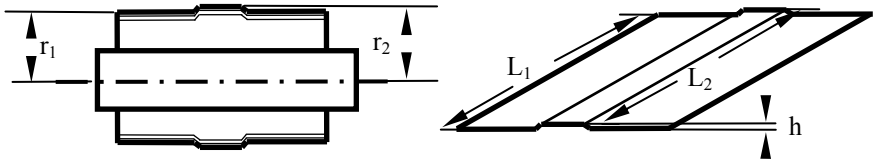

Figure 13 – Numerical transformation for baggy web.

$$h \approx r_2 - r_1 \approx \frac{L_2}{n \cdot 2\pi} - \frac{L_1}{n \cdot 2\pi} = \left(L_2 - L_1\right) \Big/ n \cdot 2\pi \qquad \{23\}$$

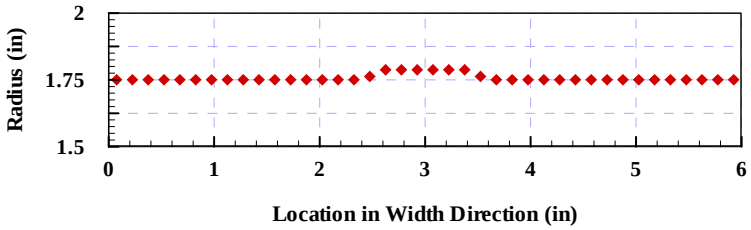

Figure 14 – Deformed shape of a wound roll after storage

The dimensional changes estimated by numerical simulation are compared favorably with measurement data. However, there are still some issues in the pseudo 3D viscoelastic winding model. Similar to most of existing winding models, the pseudo 3D viscoelastic winding model is an axisymmetric model. Asymmetric local deformation cannot be considered using this winding model. As mentioned in the previous three examples, it is assumed that the extra thickness and volume will be allocated evenly in several related laps at each location respectively. In some situations, this assumption might have resulted in errors.

Consideration of Varying Tension Histories

In this section, we investigate the effects of varying tension histories. The winding tension can be represented in terms of tension taper factor based on the work by Shelton [15] and Feiertag [16]. The code allows for easy handling of tension history in winding. Stress distribution was determined for ten different tension profiles (ranging from constant tension T_f=0 to constant torque T_f=1) for a roll wound out to 1000 laps. The number of laps can be increased based on the capacity of the computer memory.

The variations in tension and torque follow equations {24} and {25}, respectively.

$$\frac{T}{T_c} = 1 - T_f\left(1 - \frac{r_c}{r}\right) \qquad \text{(Taper of tension)} \qquad \{24\}$$

$$\frac{\tau}{\tau_c} = \frac{r}{r_c}(1 - T_f) + T_f \qquad \text{(Taper of tension by control of torque)} \qquad \{25\}$$

where r is the radius of current outer lap; r_c is the radius of core; T is tension at current lap; T_c is tension at the core; T_f is tension taper factor; τ is torque at current lap; τ_c is torque at the core.

Using on the above equations, the history of tension and torque are plotted in Figure 15 and Figure 16, respectively. Both tension and torque decrease with the increase of T_f.

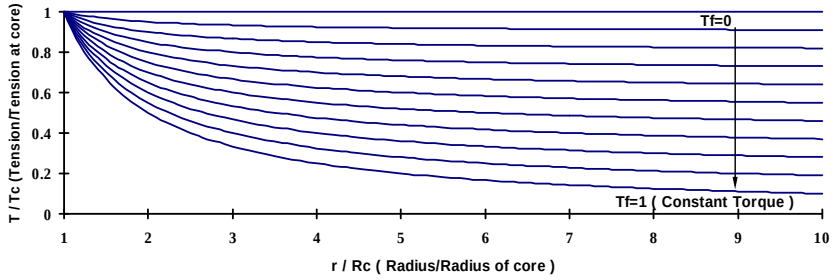

Figure 15 – Tension history

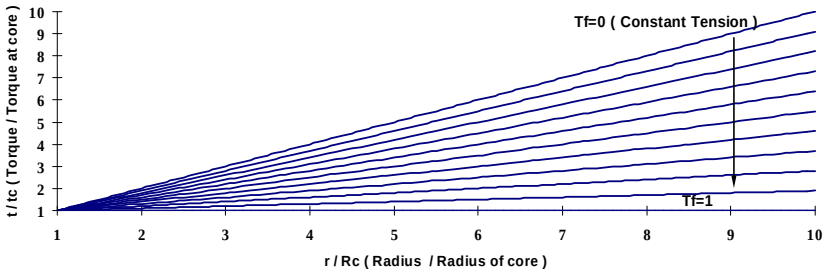

Figure 16 – Torque history

Using the pseudo 3D viscoelastic winding model, the pressure was obtained and plotted in Figure 17. The zoom-in results for ten different tension profiles are plotted in Figure 18. In Figure 18, it can be observed that the stress increases by 300% when T_f decreases from 1 to 0.

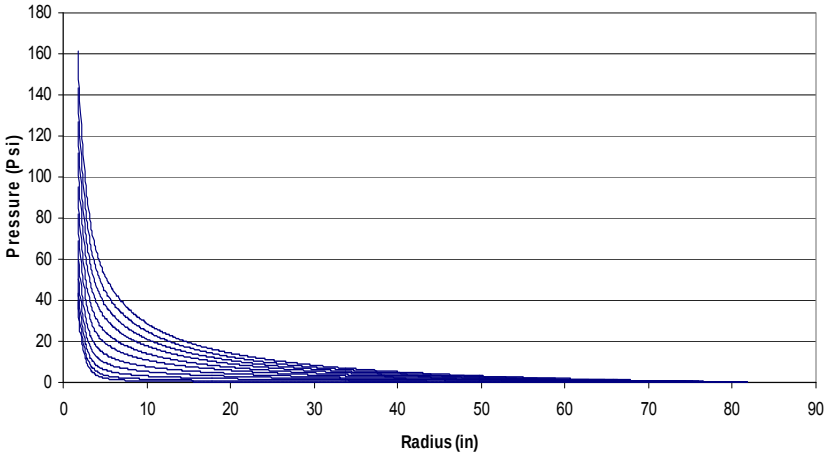

Figure 17 – Radial stress for ten different tension profiles

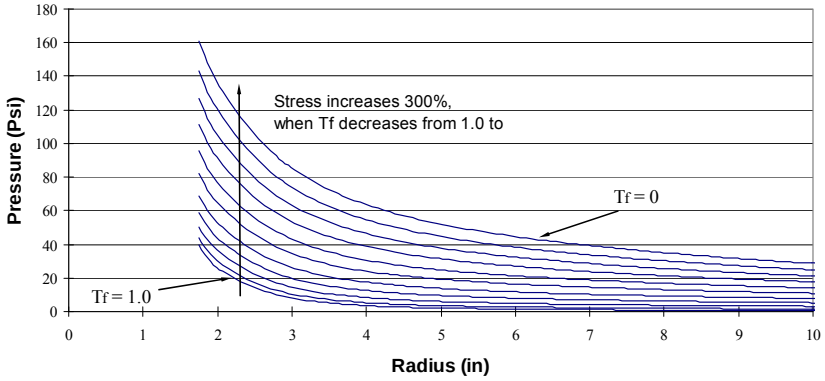

Figure 18 – Radial stress (Zoom-in) for ten different tension profiles

The initial tension used in this model is 100 psi and the tension is constant in the CMD. The results obtained right after the winding process was finished. This is a simple case we used to find the effect of winding tension variation. This method will be used to find the effect of winding tension along the time later.

CONCLUSION

A pseudo 3D winding model that has considered viscoelastic effects during winding and storage has been developed and implemented in a code. The following conclusion can be drawn.

1) The pseudo 3D transient viscoelastic winding model is capable of dealing with (1) a varying thickness profile in both MD and CMD direction; (2) a winding tension variation with the winding laps; (3) varying core stiffness in the width direction. Moreover, the viscoelastic effects built in this model allow the consideration of winding conditions, such as winding speed and tension. The model is especially suitable for viscoelastic materials with relatively short characteristic relaxation times, such as plastic webs with glass transition temperature close to room temperature.

2) The pseudo 3D transient viscoelastic winding model has been used to analyze three baggy lane problems for validation. They are (1) the formation of cambered web (in-plane imperfection) due to linearly varying thickness; and (2) the formation of localized baggy lanes due to an edge burr that resulted from slitting; and (3) the formation of a baggy web (out-of-plane imperfection) due to thickness increment in the middle of the web. Simulation results are compared with the experimental data, and reasonably good agreement was reached.

3) A pseudo 3D transient viscoelastic winding model has been developed to provide a methodology for analyzing viscoelastic winding problems of a wound roll with a finite width. The effects of varying tension history on stress distribution are considered as an example of application of the transient viscoelastic winding model.

ACKNOWLEDGEMENT

We acknowledge Prof. Bruce Feiertag for setting up the experimental facility and suggestions on conducting experiments. We thank Mr. Ronald P. Swanson for providing ideas to create controlled baggy webs for validation of the model.

REFERENCES

1. Qualls, W. R. and Good, J. K., "An Orthotropic Viscoelastic Winding Model Including a Nonlinear Radial Stiffness," Journal of Applied Mechanics, 64, 1997, pp. 201-208.
2. Hakiel, Z., "On the Effect of Width Direction Thickness Variations in Wound Rolls," Proceeding of the First International Conference on Web Handling, Oklahoma State University, Stillwater, Oklahoma, 1991, pp. 79-98.
3. Gutterman, R. P., "Theoretical and Practical Studies of Magnetic Tape Winding Tensions and of Environmental Roll Stability," General Kinetics, contract no. DA18-119-SC-42, Arlington, VA.
4. Altmann, H. C., "Formulas for Computing the Stresses in Center-Wound Rolls," TAPPI, 51(4), April 1968, pp. 176-179.
5. Pfeiffer, J. D., "Internal Pressures in a Wound Roll," TAPPI, 49(8), August 1966, pp. 342-347.
6. Pfeiffer, J.D., "Prediction of Roll Defects from Roll Structure Formula," TAPPI, 62, 1979, pp. 83-88.
7. Yagoda, H. P., "Resolution of the Core Problem in Wound Rolls," ASME Journal of Applied Mechanics, 47, 1980, pp. 847-854.
8. Hakiel, Z., "Nonlinear Model for Wound Roll Stress," TAPPI, 70(5), May 1987, pp. 113-117.
9. Tramposch, H., "Relaxation of Internal Forces in a Wound Reel of Magnetic Tape," ASME Journal of Applied Mechanics, 32, 1965, pp. 865-873.
10. Tramposch, H., "Anisotropic Relaxation of Internal Forces in a Wound Reel of Magnetic Tape," ASME Journal of Applied Mechanics, 34, 1967, pp. 888-894.
11. Lin, J. Y. and Westmann, R. A., "Viscoelastic Winding Mechanics," ASME Journal of Applied Mechanics, 56, 1989, pp. 821-827.
12. Kedl, D. M., "Using a Two Dimensional Winding Model to Predict Wound Roll Stresses That Occur due to Circumferential Steps in Core Diameter or to Cross-web Caliper Variation," Proceeding of the First International Conference on Web Handling, Oklahoma State University, Stillwater, Oklahoma, 1991, pp. 99-112.
13. Hoffecker, P., "The Analysis of A Nip Impinged, Three Dimensional Wound Roll," PhD thesis, Oklahoma State University, 2006.
14. Lee,Y.M. and Wickert,J.A., "Stress Field in Finite Width Axisymmetric Wound Rolls," Transactions of the ASME, Vol. 69, 2002, pp. 130-138.
15. Shelton, J. J., Private Communication on Tension Profiles, 2003.
16. Feiertag, B., Web Handling Seminar, Tab 4, Oklahoma State University, Stillwater, Oklahoma, 2001, pp. 4-6.
17. Swanson, R. P., "Mechanics of Non-uniform Webs," Proceeding of the Fifth International Conference on Web Handling, Oklahoma State University, Stillwater, Oklahoma,, 1999, pp. 443-459.